ANNALS OF GEOPHYSICS, 68, 2, V226, 2025; doi:10.4401/ag-9208
OPEN ACCESS

Modeling two-ways fluid-solid phase transitions in lava using Smoothed Particle Hydrodynamics

Vito Zago[1]

(1) Istituto Nazionale di Geofisica e Vulcanologia, Osservatorio Etneo, Catania, Italy

Article history: received November 20, 2024; accepted November 27, 2024

Abstract

Phase transitions are a key phenomenon in the evolution of lava flows, significantly influencing their emplacement and the formation of geological features such as lava channels and lava tubes. Here, a numerical model employing Smoothed Particle Hydrodynamics (SPH) to simulate two-way phase transitions between solid and fluid states in lava is presented. By accurately representing the solidification dynamics and incorporating a temperature range that accounts for the solidus and liquidus temperatures, the model addresses limitations in previous approaches that relied on oversimplified phase transition assumptions. We validate the model against Stefan's benchmark test case and apply it to two illustrative volcanic scenarios using artificial volcanic-like environments, demonstrating how the model effectively captures the processes of solidification and fusion within the modeled lava flow. The results underscore the importance of phase transition modeling in understanding the complex behavior of lava flows in real-world volcanic contexts.

Keywords: Phase transition; Mixtures; SPH; Lava tube; Stefan

1. Introduction

Lava flows are inherently temperature-dependent phenomena. Temperature plays a fundamental role in the flow dynamics, shaping both how it behaves and when it eventually halts. One key factor of this dependence is the influence of temperature on the viscosity. Higher temperatures reduce viscosity, making lava more fluid and allowing faster flow. Yet, a fundamental aspect of the thermal nature of lava flows is the occurrence of phase transitions. Solidification of lava is not just the final stage of the flow, but phase transitions actively influence the ongoing behavior of the flow and thus its emplacement. Solidification along the flow margins can form levees that channelize the lava (Dietterich and Cashman, 2014), while solidification at the front can partially or completely stop its advance. Solidified lava can also enclose the flow, forming lava tubes (Calvari and Pinkerton, 1999) which act as thermal shield and can allow the lava to travel greater distances, extending the area of emplacement. Conversely, fusion can open new pathways or widen existing channels (Kauahikaua et al., 1998). Phase changes thus introduce considerable complexity into the modeling of lava flows, highlighting the importance of detailed temperature-dependent simulations. Effective lava flow models must account for temperature and its effects on flow dynamics, as these factors are essential for understanding and predicting the behavior of lava in real-world scenarios (Cordonnier et al., 2016).

Among the many numerical models used to simulate lava flows, the Smoothed Particle Hydrodynamics (SPH) method has been considered to produce accurate and highly detailed simulations (Hérault et al., 2011; Zago et al., 2018). Models based on SPH have proven effective in considering both rheological and thermal aspects of fluids, as well as their interplay. Phase transitions have been considered in SPH models for lava (Hérault et al., 2011, 2010; Zago et al., 2018), primarily from a thermal point of view, so to keep into account the latent heat during solidification and its effects on viscosity through the resulting temperature evolution. The resulting viscosity acts in turn on the dynamics of the flow. In these works, the implementation of phase transitions is optimized for solidification, utilizing a simplified physics that adopts a single transition temperature. This can be appropriate for pure materials, but it is not adequate for mixtures, such as lava. In this case, the varying melting temperatures of the constituent elements determine partial phase transitions occurring over a range of temperature, defined by the solidus temperature (T_s) and the liquidus temperature (T_l). For temperatures below T_s the phase changing material (PCM) is entirely solid, and above T_l it is entirely liquid. Within the range, both phases coexist, resulting in the formation of a *mushy* region (Groulx and Ogoh, 2010). The work of Monaghan (2005), takes into account a more complete description of the phase transition modeled with SPH, which is focused on ice and salty solutions. From a mechanical perspective, the approximation of solidification using high viscosity presents challenges (Hérault et al., 2011; Zago al., 2018; Bilotta et al., 2022), as a viscous fluid, regardless of its viscosity, behaves differently from a solid. On the other hand, high viscosities can introduce stiff terms in the governing equations, complicating the numerical integration process and often necessitating more complex integration schemes (Bilotta et al., 2022; Zago et al., 2018). Consequently, it is essential to address the mechanical transition from solid to liquid. The SPH model proposed by Fuchs et al. (Fuchs et al., 2021) gives an example of solidification by modeling the mechanics of groups of solidified particles as rigid bodies. However, this model also adopts a single temperature threshold and ignoring the formation of a mushy region.

Here, we developed a model for phase transitions in mixtures that can accurately simulate both solidification and fusion, exploring its potential applications in lava flow simulations. The model offers an enhanced treatment of the thermal behavior of phase transitions, by considering a temperature range and phase-dependent parameters. Additionally, we analyzed the mechanical aspects and present a method for the transformation between solid and liquid phases. The model was validated against Stefan's test case, and we show some examples of its applications in a volcanic context.

2. The model

The dynamics of the fluid is modeled according to the Navier-Stokes momentum equation:

$$\rho \frac{D\mathbf{u}}{Dt} = -\nabla P + \nabla \cdot (\mu \nabla \mathbf{u}) + \mathbf{G}, \tag{1}$$

where $\boldsymbol{u}$ indicates velocity, P pressure, μ the dynamic viscosity, and $\mathbf{G}$ represents external forces, which in this case will only account for gravity. We model the evolution of the density ρ by means of the continuity equations for mass:

$$\frac{D\rho}{Dt} = -\rho \nabla \cdot \mathbf{u}. \tag{2}$$

We link the two equations above by using an equation of state, which gives the pressure as a function of density (Cole, 1948):

$$P(\rho) = c_0^2 \frac{\rho_0}{\gamma} \left(\left(\frac{\rho}{\rho_0} \right)^{\gamma} - 1 \right), \tag{3}$$

where ρ_0 is the density at rest (at ambient pressure), c_0 the speed of sound and γ the polytropic constant.

Thermal conduction is described by means of the heat equation:

$$\rho\, c_p \frac{DT}{Dt} = \nabla(\kappa \nabla T), \tag{4}$$

where T is the temperature, c_p is the specific heat at constant pressure and κ is the thermal conductivity. Because of our focus on the phase transition mechanism, we neglect the heat exchange at the surface due to radiation and air convection (Zago et al., 2018).

2.1 The SPH discretization

To numerically solve the governing equations introduced above, we adopt the Smoothed Particle Hydrodynamics (SPH) method (Gingold and Monaghan, 1977; Lucy, 1977). This is a Lagrangian and mesh-free method, which has proven to be effective for the simulation of free surface flows undergoing large deformations (Monaghan, 1994), such as lava flows (Hérault et al., 2011; Zago et al., 2017; Zago et al., 2018; Zago et al., 2018). In the SPH method the continuum is discretized with a finite set of volumes, called particles, each carrying physical and chemical information about the represented volume of fluid, such as velocity, density, mass, temperature. The basis of the method relies on the SPH smoothing, that is the way in which particle properties are interpolated from the values at the neighbors, weighted by a radially decreasing function, called smoothing kernel, $W(r,h)$. Here, r indicates the distance from the neighbouring particle and h is a parameter called smoothing length. The smoothing kernel is usually chosen with a compact support, which radius is called influence radius, usually determined as a multiple of h. For the simulations presented in this work we adopt a Wendland kernel (Wendland, 1995; Zago et al., 2021), defined as $W(r,h) = \widetilde{W}\left(\frac{r}{h}\right)$ and $F(r,h) = \tilde{F}\left(\frac{r}{h}\right)$ with:

$$\widetilde{W}(q) = C_W(2q+1)\left(1-\frac{q}{2}\right)^4 \qquad 0 \le q \le 2; \tag{5}$$

where, working in two dimensions, $C_w = \frac{7}{4\pi h^2}$ and $C_F = C_w \frac{5}{8h^2}$.

A fundamental property of SPH is then the interpolation of gradients, which allows to discretize the spatial derivatives in the governing equations. This allows to obtain the gradient of the physical quantities based on a summation of the values over the surrounding neighbors, weighted by the gradient of the smoothing kernel, which is a known function.

Given a particle i and a neighboring particle j, and considering the symmetry of the SPH smoothing kernel W, the gradient of the kernel can be written as:

$$\nabla_i W_{ij} = -\frac{\boldsymbol{x}_{ij}}{|\boldsymbol{x}_{ij}|}\frac{\partial W(r,h)}{\partial r}\Big|_{r=|x_{ij}|}, \tag{6}$$

where $\boldsymbol{x}_{ij} = \boldsymbol{x_i} - \boldsymbol{x_j}$, and h is the kernel smoothing length. By choosing a kernel for which

$$F(r) = \frac{1}{r}\frac{\partial W}{\partial r}, \tag{7}$$

has an analytical expression, and given $F_{ij} = F(|\mathbf{x}_{ij}|)$, we can then write

$$\nabla_{ij} W_{ij} = -\mathbf{x}_{ij} F_{ij}. \tag{8}$$

$$\tilde{F}(q) = C_F(q-2)^3 \tag{9}$$

2.2 SPH discretization of the equations

The governing equations presented at the beginning of the section can be discretized according to the SPH method (Zago et al., 2017) obtaining:

$$\frac{D\boldsymbol{u}_i}{Dt} = \sum_j \left(\frac{P_i}{\rho_i^2} + \frac{P_j}{\rho_j^2}\right) F_{ij} m_j \boldsymbol{x}_{ij} - \sum_j \frac{2\bar{\mu}_{ij}}{\rho_i \rho_j} F_{ij} m_j \boldsymbol{u}_{ij} + \boldsymbol{g}, \tag{10}$$

for the momentum Eq. (1), where $\bar{\mu}_{ij}$ is the harmonic mean of the viscosities of the two particles i and j, and

$$\frac{D\rho_i}{Dt} = -\sum_j \boldsymbol{u}_{ij} \boldsymbol{x}_{ij} F_{ij} m_j + \xi h c_0 \sum_j \boldsymbol{\psi}_{ij} F_{ij} m_j, \tag{11}$$

for the continuity Eq. (2). The second term in the summation is the artificial density diffusion (Molteni and Colagrossi, 2009; Antuono et al., 2012) introduced in order to remove high-frequency oscillations from the density field. The term ξ is a weighting factor for the density diffusion that we take $\xi = 0.1$, and the $\boldsymbol{\psi}_{ij}$is defined as:

$$\boldsymbol{\psi}_{\mathrm{ij}} = \begin{cases} 2\left(\dfrac{\rho_i}{\rho_j} - 1\right), & \dfrac{|P_i - P_j|}{\rho_i g |y_i - y_j|} > 1 \\ 0, & otherwise. \end{cases} \tag{12}$$

The thermal Eq. (3) is discretized as (Zago et al., 2018):

$$\frac{DT_i}{Dt} = -\frac{1}{\rho_i c_p} \sum_j \frac{2 m_j k_{ij} T_{ij}}{\rho_j} F_{ij}, \tag{13}$$

where k_{ij} is the harmonic mean of the thermal conductivity of the two particles i and j.

2.3 Model for phase transitions

When modeling the phase transition between solid and liquid phases, we must consider the thermal behavior of the particles. Specifically, how their temperature evolves according to the heat transfers, and the changes in their mechanical properties.

The phase transition model presented here constitutes an advancement over previous SPH approaches developed for lava flow simulation (Hérault et al., 2011; Zago et al., 2018; Zago et al., 2018). In those studies, the thermal behavior of lava is simplified, assuming a single transition temperature (as for pure materials), and the temperature remains constant during phase transition until the entire latent heat, L, is transferred. The more realistic model adopted here, includes solidus and liquidus temperatures (T_s and T_l, respectively) which are common of mixtures, such as lava. The phase transition occurs between these two temperatures, where both liquid and solid phases coexist, with different component transitioning at different times. During this transition, a portion of the transferred heat is absorbed as latent heat of the component undergoing transition, while another portion determines the temperature to evolves between the two values.

The phase transition model in (Hérault et al., 2011; Zago et al., 2018; Zago et al., 2018) keeps track of the fraction of exchanged latent heat separately from the temperature integration. Such approach is tightly linked to the single transition temperature making it less straightforward when incorporating bot solidus and liquidus temperatures.

Here we model the effect of latent heat by using an apparent heat capacity. Within the temperature interval $[T_s, T_l]$, the heat capacity, c_p, is modified as:

$$\bar{c_p} = c_p + \frac{L}{T_l - T_s} \tag{14}$$

where the additional term accounts for the heat absorbed and released by the material as latent heat.

From a mechanical perspective, the fusion process involves transforming solid particles into fluid particles, while vice-versa, solidification leads fluid to become solid particles. The transition from solid to fluid is straightforward: an SPH solid particle, initially arranged in an ordered lattice, is converted to a fluid particle and becomes free to move. Its dynamics are then determined by the computed hydrodynamic interaction forces. On the other hand, the transition from fluid to solid necessitates a more careful treatment. Directly converting a fluid particle into an SPH solid particle would freeze it in place and prevent it from flowing with the surrounding fluid. This behavior is acceptable for particles turning solid in proximity of a solid boundary and creating a coalescence with the levees at a position which remain fixed over time. However, it would create an artifact for particles becoming solid on the surface of the flow. This condition introduces a level of detail which goes beyond the mechanism of the phase transition, which is the primary focus of this paper, and of the 2D model presented here. Consequently, the aspect of surface solidification is left outside the scope of the present work.

As for the mushy region, mechanical behavior of the material in such state depends on the ability of the solid fraction to maintain structural integrity and the forces applied, which can rip off the mushy part as soon as sufficiently soft. To adopt a conservative approach, we assume that the type of a particle's type, solid or fluid, only changes when a complete phase transition has occurred. Specifically, a fluid particle is converted to a solid particle only when its temperature drops below the solidus temperature, and a solid particle switches to a fluid particle only when its temperature rises above the liquidus temperature. Adjustments can be made to assume a more realistic behavior, allowing the particle type to toggle when the temperature moves outside a narrower interval within the thermal phase transition range.

2.4 Boundary conditions

In SPH, boundary conditions are typically obtained by using particles, called boundary particles, that impose their conditions (velocity, temperature, etc.) on the fluid particles, and ensure completing the support of the kernel at the edges of the fluid-solid interfaces. There are many conventions to implement this in detail, we use the *dynamic boundary* model (Crespo et al., 2007; Bilotta et al., 2022). In this model, layers of boundary particles are placed along the theoretical border at intervals of Δp, starting from the exact theoretical position and going outwards with respect to the domain. These particles are assigned the theoretical velocity of the border (typically zero, for fixed walls) and their density evolves as for fluid particles, according to the equation of continuity (2).

To generate an inlet flow we adopt open boundaries (Zago, 2019). Similarly to the dynamic boundary model, we implement open boundaries by using layers of particle, so to give continuity to the domain. These particles are placed in the so-called buffer region, that gives the shape to the inlet. The velocity of the particles in the buffer region is imposed as a function of time and space, to create a flow inlet with a time-dependent velocity profile. When one of these particles crosses the edge of the buffer region, it is converted to a fluid particle and is let free to evolve within the domain as a generic fluid particle. A new buffer particle with identical properties is created at the opposite edge of the buffer region to sustain the inlet flow.

2.5 Integration scheme

We use an explicit second order integration scheme, previously adopted for lava simulations (Hérault et al., 2011; Zago et al., 2017). As an explicit scheme, it requires stability conditions on the maximum allowed time step. We adopt CFL-like conditions (Zago et al., 2018), according to which the time step should satisfy:

$$\Delta t_\beta \leq \min\left\{ C_1 \sqrt{\frac{h}{\|\mathbf{a}_\beta\|}}, C_2 \frac{h}{c_\beta}, C_3 \frac{\rho_\beta h^2}{\mu_\beta}, C_4 \frac{\rho_\beta c_p h^2}{\kappa} \right\}, \tag{15}$$

where $\mathbf{a}_\beta$ is the acceleration of the particle β, c_β is the speed of sound at density ρ_β, and C_1, C_2, C_3 and C_4 are stability constants. We use $C_1 = C_2 = 0.3$, $C_3 = 0.125$ and $C_4 = 0.1$ (Zago et al., 2018). About the thermal condition, we use the value of nominal heat capacity (as opposed to the apparent heat capacity $\overline{c_p}$), as it gives faster thermal diffusion, which is the limiting aspect for the time step. The maximum allowed time step for the whole system is then the minimum time step over all particles, $\Delta t = \min_\beta \Delta t_\beta$.

Because of these constraints, the speed of sound adopted for SPH simulations is usually taken smaller than the physical one, but still high enough to prevent a compressible behavior. A condition of Weak compressibility is achieved if the speed of sound is sufficiently high to constrain density variations within a limited range. We use ten times the maximum velocity developed in the simulation, considering also the hydrostatic velocity from the Torricelli theorem:

$$v_h = \sqrt{2gh}, \tag{16}$$

where g is the magnitude of gravity, and h is the maximum depth of the fluid.

Being the focus of this work the methodical aspect of the model, for the sake of code clarity we do not consider at this stage the numerical improvements adopted in previous SPH models for lava flows (Hérault et al., 2011; Bilotta et al., 2022; Zago, Bilotta et al., 2020). The code is written in Python language, using double numerical precision.

3. Model validation

We verify the phase transition model by reproducing Stefan's problem. A block of phase changing material (PCM) is placed in contact with a thermal source which sustains the phase transition. A phase transition front between the two phases propagates through the PCM body, and the numerical model is verified according to the ability to correctly reproduce this propagation over time. For a pure elements PCM, the phase transition happens entirely at a well-defined temperature and the position of transition front can be well identified.

This position can be expressed analytically as (Hérault, 2008):

$$x_t(t) = 2\lambda\sqrt{\alpha t} \tag{17}$$

where λ is called similarity variable, and is the solution of the equation:

$$T_t - T_0 = \mathrm{erf}(\lambda)\, e^{\lambda^2} \left(\frac{\lambda L \sqrt{\pi}}{c_p} + \frac{(T_t - T_0) e^{-\lambda^2}}{\mathrm{erfc}(\lambda)} \right). \tag{18}$$

Here, T_t is the temperature at which the transition happens, and T_0 is the initial temperature of the PCM. We set up the Stefan's test case with the PCM at its liquid state and model the solidification process, using a setup similar to that of Hérault (2008). In the case of mixtures, a mushy region is present between the two phases, preventing a straightforward comparison with the analytical solution. We therefore address the comparison by considering the transition front at the edge of the mushy region where the PCM completes the phase transition and becomes solid. With this choice, we mark the phase transition at the point where the entire latent heat has been gained (fusion) or lost (solidification), which is conceptually similar with the transition for single materials. In such case it is important that the T_t temperature in Eq. (18) coincides with the solidus temperature of the material.

We set up a Stefan test case where the PCM is a 1 meter wide square block, discretized with 80 SPH particles over its length, and the thermal source is obtained with four layers of boundary particles placed at the left of the PCM. We set the origin of the x axis in correspondence of the boundary particle closest to the PCM. To act as a thermal source, the temperature of these particles is kept constant over time at a value T_w, and so $T(x,t) = T(0,t) = T_w$. We use unitary values for density ρ, heat conduction k, specific heat c_p, and latent heat L. The initial temperature of the PCM is $T_0 = 1.2$ K and, for simplicity, we assign a value to the similarity variable $\lambda = 0.5$, which requires $T_w = 0.190602$ K. We assign solidus and liquidus temperatures as respectively $T_s = 1$ K and $T_l = 1.05$ K. Figure 1 shows the simulation domain at simulated time t = 0.1 s. The left image (a) indicates the different components of the domain. The mushy region is identified by the particles whose temperature is in the range $[T_s, T_l]$.

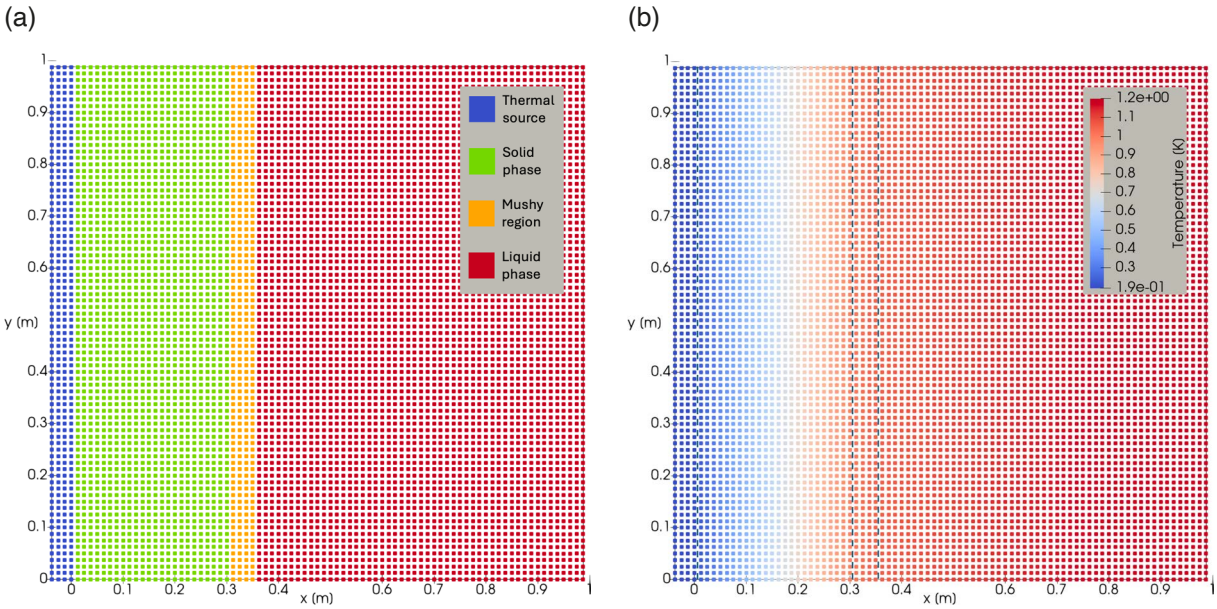

Figure 1. SPH simulation of Stefan's problem at t = 0.1 s. (a) particles are colored by type: thermal source (blue), the solidified PCM (green), the mushy region (yellow) and the still liquid PCM (red). (b) the corresponding temperature; dashed lines are a reference to the regions shown in (a).

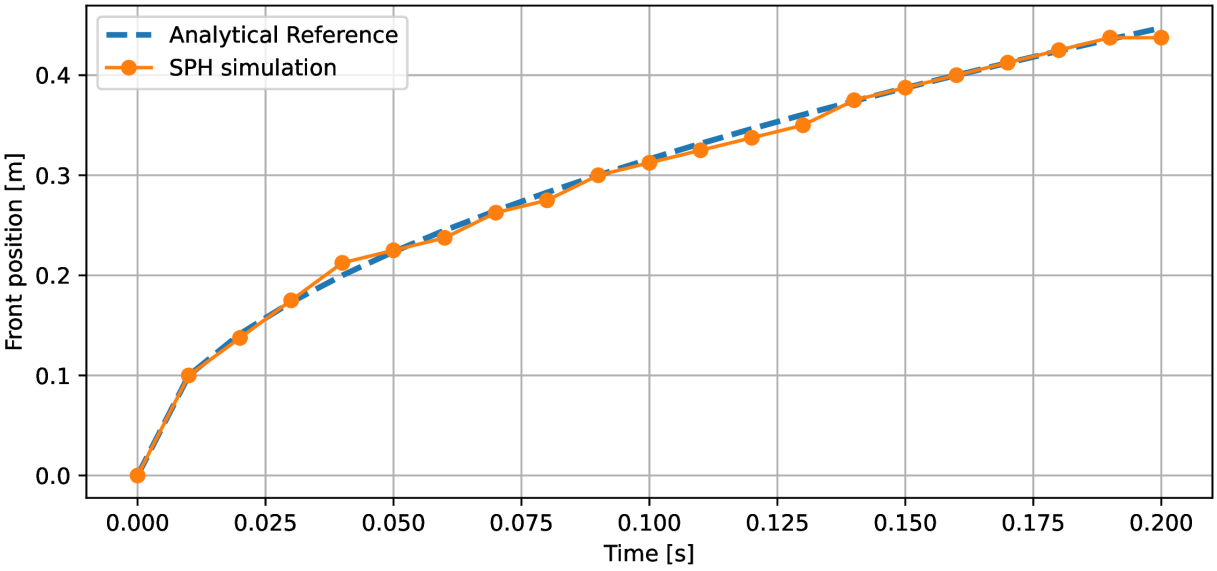

Figure 2. Position of the fusion front over time (blue: analytical, orange: SPH simulation).

The graph in Fig. 2 shows the position of the solidification front over time, indicating a good agreement between the simulated and the analytical results. Small deviations from the analytical curve are due to the spatial discretization, as in this problem particles are fixed in space, and the advancement of the phase transition is tracked across the layers of particles. Although the model has been verified for a solidification case, the definition of the apparent heat capacity, upon which the phase transition depends, can keep track of both gained and lost heat. This test can thus be generalized to both directions of phase transition.

4. Model testing

In this section, we apply the model to a simulation setup that mimics some characteristics of volcanic environments. These tests are mostly illustrative, to show the occurrence and development of both ways of phase transition.

4.1 Simulation setup

We use the geometry shown in Fig. 3a. This setup has no specific real-world reference and was manually created. The particle set (Fig. 3b) is generated by intersecting a regular grid of particles with the black areas of the sketch. Here we remark the ease of handling complex topographies with SPH. Geometries can be defined by placing particles and assigning their properties, and no analytical conditions or forms of interconnections are required.

The setup is inspired by a lava tube with skylights, enabling the study of various forms of fluid-solid interactions, including the common interactions with the ground, and with walls as seen in lava flowing through a tunnel. The domain is 99 m long and 35 m high, and is discretized with a spatial step $\Delta p = 0.5$ m.

The specific geometry allows a flow diversion at the upper skylight that exposes part of the ground to the inner core of the lava flow, along with regions where flow stagnation occurs.

Although this is an illustrative example, we tend to assign a realistic set of thermal parameters which are relevant to the focus of this work. We use values similar to those adopted in Zago et al. (2018): heat capacity: $c_p = 2400$ J/K, latent heat $L = 350$ kJ/kg, solidus temperature $T_s = 1000$ K, liquidus temperature $T_l = 1200$ K and effusion temperature $T_e = 1350$ K. We apply also different thermal conductivity for liquid and solid phases: $k_l = 2.0$ W/(m×K) and $k_s = 1.15$ W/(m×K).

About the other physical properties, and mostly for those governing the motion of the fluid, we apply some arbitrariness in selecting the values, that are meant to reproduce flow conditions favorable for a proper utilization of the designed topography and the development of phase transitions. Referring to (Zago et al., 2018), we use a temperature-dependent viscosity, given by:

$$\mu(T) = 500 \exp\left(10, -1.0 + \frac{1}{T - 610}\right), \tag{19}$$

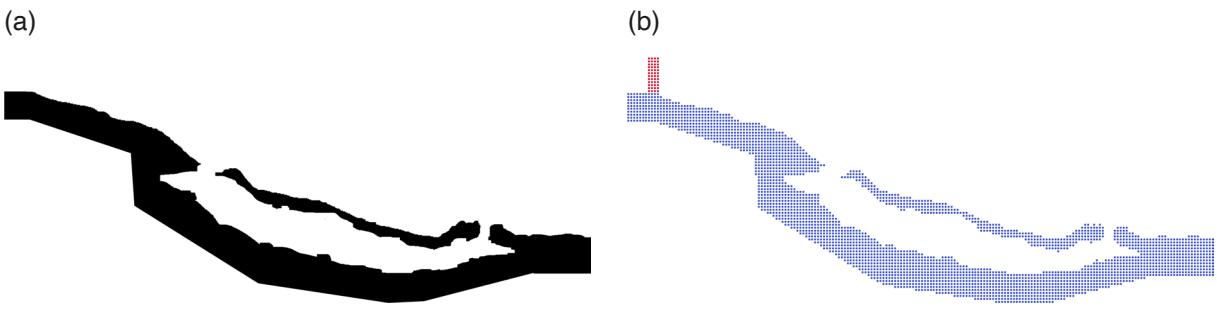

Figure 3. Setup for model test, synthetic geometry of a representative lava tube. Vertical profile of a lava tube. (a) the original geometry; (b) the SPH discretization. Blue particles are directly created from the given geometry, the red particles implement the buffer region of the inlet (see Subsection 2.2).

and we use a unit value for density, so to enhance thermal diffusion, allowing for the rapid development of illustrative phase transitions within relatively short simulations.

The flow is generated through an inlet, implemented using open boundaries (Subsection 2.2). As illustrated in Fig. 3b, the inlet (red particles) is positioned at the top of the uphill region and extends 6 m in height. We generate the flow with a linear velocity profile, similarly to a Couette flow, with maximum velocity at the top particle set to $v_s = 1.5$ m/s. The linear profile is designed to ensure zero velocity at the boundary particle right below the buffer region.

4.2 Simulation results

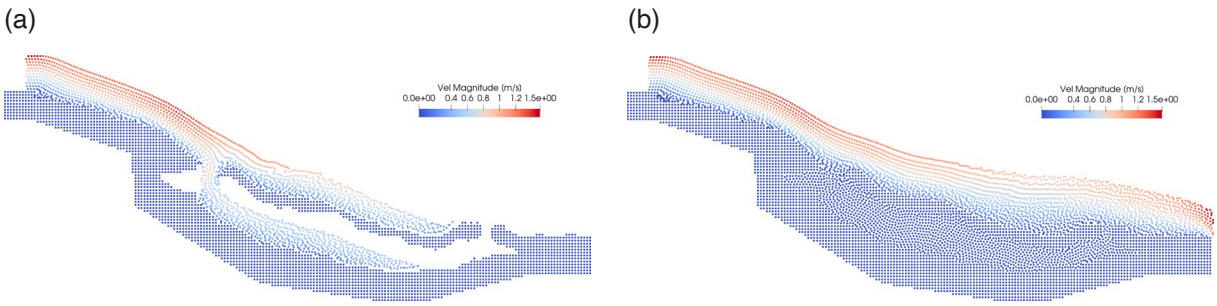

Figure 4. (a) simulation at time $t = 100.0$ s; (b) simulation at $t = 514.0$ s. Particles are colored by module of velocity.

4.2.1 First case: solidification

Figure 4 shows two instants of the simulation. The flow, generated at the inlet, flows down the ground and completely fills the tube-like cavity. Because of the thermo-mechanical properties of the fluid, the flow is almost static within the cavity (Fig. 4b). We notice that the stream-like patterns observed in on the surface and at the diversion are an artifact of high viscosity, which contrasts particle disordering and preserves the artificial initial discretization along the short and quite regular path from the inlet. This effect is further amplified by the two-dimensional nature of the flow, which constrains particle movement within the plane, reinforcing this ordered structure. The extent of this phenomenon is, however, influenced by the spatial resolution, as smaller particle sizes reduce its impact on the overall flow. However, given the illustrative purpose of this study and the need for clear visualization, finer discretizations are not pursued.

Figure 5 shows the temperature at time at $t = 514.0$ s, while Fig. 6 shows only the boundary particles (i.e. solid particles) at the same instant. Particles marked in red are those that have transitioned from liquid to solid during the simulation.

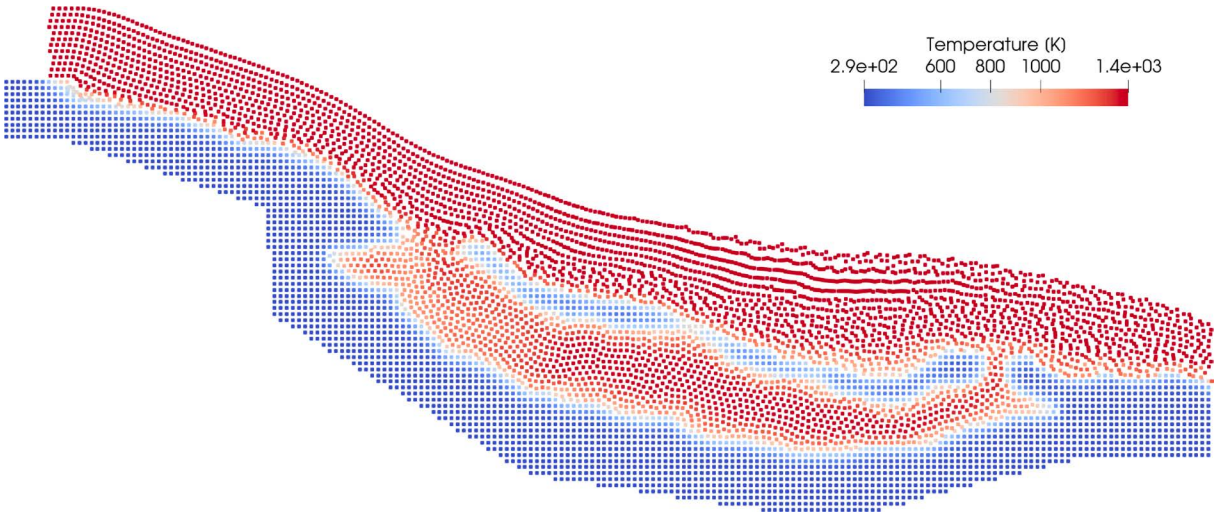

Figure 5. Simulation at $t = 514.0$ s. Particles colored by temperature.

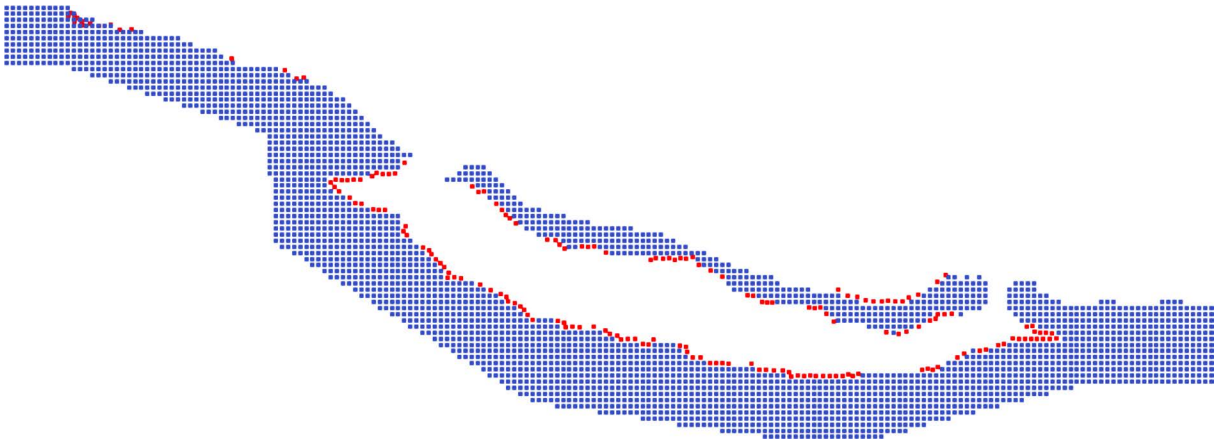

Figure 6. Simulation at $t = 514.0$ s. Only border. Particles in blue are the original particles, those in red are the particles aggregated after solidification.

4.2.2 Second case: fusion

To test also fusion, we setup a new simulation and assume different fluid properties which favor heat conduction to the ground and involve lower latent heat for the phase transition. We therefore use heat capacity $c_p = 1000$ J/K, latent heat $L = 100$ kJ/kg, solidus temperature $T_s = 1000$ K, liquidus temperature $T_l = 1100$ K and effusion temperature $T_e = 1500$ K, and thermal conductivity for liquid and solid phases: $k_l = 2.0$ W/(m×K) and $k_s = 1.15$ W/(m×K).

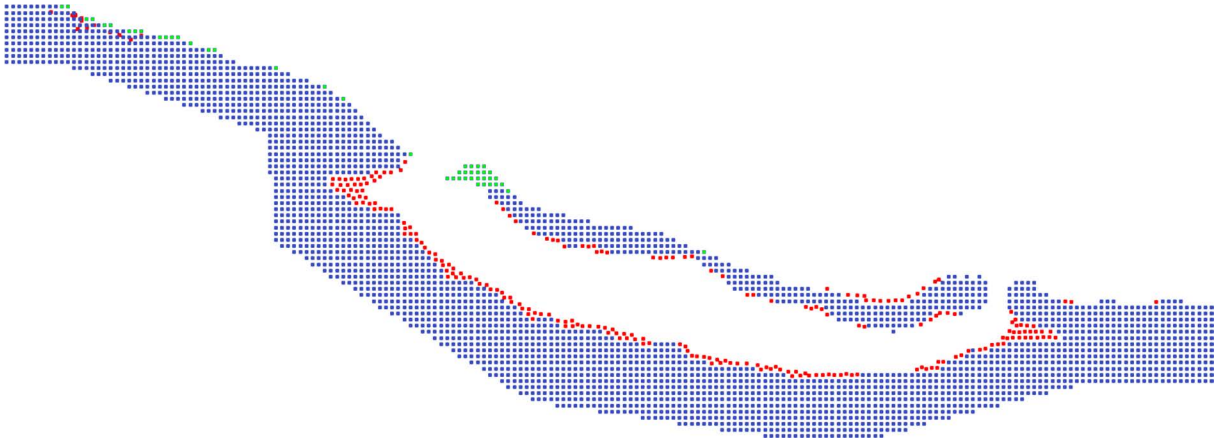

Figure 7. Simulation at $t = 850.0$ s. Only border. Particles in blue are the original particles, those in red are the particles aggregated after solidification and green particles indicate the region melted during the simulation.

Figure 7 shows the status of the solid particles for this second configuration, indicating both particles that were added during the simulation due to solidification and the place of solid particles that were removed due to fusion.

5. Discussion

SPH models offer a detailed representation of flow dynamics and are valuable tools for studying the complex physical phenomena occurring within fluid flows (Zago et al., 2023). The introduction of an accurate model for phase transition enhances our understanding of flows, particularly for fluids that are highly temperature-dependent, such as lava.

The simulations presented above offer a comprehensive view of the flow parameters, including velocity and temperature (Figs. 4 and 5) and illustrate their relationship with the phase transitions (Figs. 6 and 7). These results highlight the correlation between areas where the flow is slower or stagnates and the regions where the fluid cools and solidification occurs, leading to coalescence with the walls. On the other hand, the simulations also demonstrate that under favorable thermal properties and flow conditions, fusion of solid regions can occur (Kauahikaua et al., 1998). Figure 7 shows that fusion is particularly prominent in areas directly exposed to the main flow of fresh lava, where a persistent heat supply is maintained, such as in the sloping region near the inlet and at points of diversion of the flow, allowing closer proximity to the hotter interior of the main flow. While these simulations showcase the potentiality of the model, it is important to note that the assumptions made regarding density may affect the realism of the time scales associated with lava advection and thermal conduction. To address this limitation, the timescale of advection can be adjusted to serve as a rapid representation of an equivalent, slower flow.

An advantage of adopting the effective heat capacity approach is its ability to track the evolution of a mushy region, as shown in Section 3. This allows for the observation of both solid and liquid phases undergoing a phase transition within the domain. The mushy region is treated solely from a thermal perspective, ensuring that temperature evolution and associated heat exchanges are accurately represented. However, changes in the resistance of the material are not directly modeled, nor is the resistance to surrounding fluid flow, which could lead to material erosion through mechanisms beyond phase transition, such as drag. In this model, the mechanical phase transition – where SPH particles transition from boundary to fluid – is triggered at the liquidus temperature, once the full latent heat has been transferred. Additionally, earlier detachment of material can be indirectly accounted for by allowing the mechanical phase transition to occur at a specific temperature within the melting range.

As introduced in Section 2.3, solidification poses noticeable challenges from a mechanical perspective. When considering particles in contact with the ground, they can become ordered within the lattice according to the flow conditions. In scenarios of slow and ordered flow, particles tend to settle into a hexagonal structure. However, for flows with higher dynamics, solid particles often do not align with the existing structure of the boundary particles, leading to highly disordered growth of the boundaries. This drawback can be avoided by designating a particle as "thermally solid" once its temperature drops below T_s. This designation allows thermal properties dependent on the PCM state to be accurately applied. The particle is then converted to an actual boundary particle when it is within a distance Δp of another boundary particle. This approach ensures that the thermal shielding provided by the solidified crust is active through the thermally solidified particles, which subsequently aggregate mechanically to the boundaries once the proximity requirement is satisfied. More advanced forms of particle aggregation can be achieved by allowing solidifying particles to mutually aggregates and form floating rigid bodies, as presented by Fuchs et al. (Fuchs et al., 2021). This approach can incorporate the mechanical properties of the mushy region, suggesting the potential for coupling with solid continuum mechanics methods. Moreover, this paper primarily introduces the phase transition and presents a 2D mechanical framework, which serves as a foundation for preliminary studies. Extending this model to three dimensions would facilitate more comprehensive studies and require a more thorough treatment of the mechanics involved.

Despite ongoing advancements (Hérault et al., 2010), high-resolution computational methods capable of accurately reproducing the complexities of lava flows remain largely theoretical and are seldom used in real-time modeling of ongoing events. In these cases, simpler, faster and lower-resolution models are typically favored for their efficiency. However, it is crucial to continue developing detailed approaches from both theoretical and methodological perspectives, as these efforts lay the groundwork for a future where computational capabilities can meet the demands of such complex modeling. This trend has already been observed with high-resolution computational methods, including SPH. Initially formulated in the latter half of the twentieth century, SPH has gained relevance in recent decades with the advent of parallel computing, which enables the processing of large computational loads that were previously impractical (Hérault et al., 2010). Furthermore, the current emergence and consolidation of innovative computational paradigms, such as AI-driven emulators (Amato, 2024) and quantum computing (Au-Yeung et al., 2024), holds promise for making even the most computationally demanding methods feasible. As these technologies mature, they have the potential to operationalize high-fidelity models, bridging the gap between theoretical accuracy and practical applicability.

6. Conclusions

This works has presented a novel SPH model for simulating two-way phase transitions between solid and liquid phases in mixture materials, such as lava. The model effectively incorporates the solidus and liquidus temperature, allowing a detailed tracking of the formation of mushy regions, a critical aspect in understanding the behavior of lava flows under varying thermal conditions. The accuracy of the model has been validated against a standard benchmark for phase transitions, specifically Stefan's problem, showing strong consistency with the analytical solutions. Following this validation, the model was applied to two test cases inspired by volcanic settings, each designed to represent a range of flow conditions influenced by phase transitions. These tests showed the effectiveness of the model in reproducing realistic lava simulations, highlighting its ability to capture essential thermo-mechanical aspects of the flow.

The detailed analysis facilitated by the SPH method allows for a comprehensive examination of how phase transitions affect flow dynamics, including solidification and fusion processes. This level of detail is crucial for accurately modeling lava behavior in real-world scenarios, where temperature variations can lead to complex interactions between solid and liquid phases.

The model introduced here constitutes a fundamental building block for future SPH-based lava models, paving the way for a more accurate representation of the intricate behaviors associated with phase transitions. As computational capabilities advance, the integration of this model into larger, high-resolution simulations will be vital for predicting volcanic activity and understanding the dynamics of lava flows in greater detail.

The advancement of this SPH model not only contributes to the theoretical understanding of phase transitions in lava but also has significant practical implications for volcanic risk assessment and management. Future work should focus on extending the model to three dimensions and incorporating additional factors such as real topographies and the influence of external environmental conditions. By doing so, we can enhance our predictive capabilities and improve our responses to volcanic events, ultimately contributing to better hazard mitigation strategies.

References

Amato, E. (2024). Enhancing Computational Fluid Dynamics with Artificial Intelligence: an AI-based Smoothed Particle Hydrodynamics (SPH) Emulator for Lava Flow Modeling, Ph.D. Thesis, University of Palermo, https://hdl.handle.net/20.500.14242/172361.

Antuono, M., A. Colagrossi and S. Marrone (2012). Numerical diffusive terms in weakly-compressible SPH schemes, Comput. Phys. Commun., 183, 12, 2570-2580, doi:10.1016/j.cpc.2012.07.006.

Au-Yeung, R., A. J. Williams, V. M. Kendon and S. J. Lind (2024). Quantum algorithm for smoothed particle hydrodynamics, Comput. Phys. Commun., 294, 108909, doi:10.1016/j.cpc.2023.108909.

Bilotta, G., V. Zago, V. Centorrino, R. A. Dalrymple et al. (2022). A numerically robust, parallel-friendly variant of BiCGSTAB for the semi-implicit integration of the viscous term in Smoothed Particle Hydrodynamics, J. Comput. Phys., 466, 111413, doi:10.1016/j.jcp.2022.111413.

Bilotta, G., V. Zago, A. Hérault, A. Cappello et al. (2024). Optimization of flexible neighbors lists in Smoothed Particle Hydrodynamics on GPU, Adv. Eng. Softw., 196, 103711, doi:10.1016/j.advengsoft.2024.103711.

Bilotta, G., V. Zago, A. Hérault, H. D. van Ettinger et al. (2023). Fast, feature-rich weakly-compressible SPH on GPU: coding strategies and compiler choices, arXiv:2207.11328, arXiv. http://arxiv.org/abs/2207.11328.

Calvari, S. and H. Pinkerton (1999). Lava tube morphology on Etna and evidence for lava flow emplacement mechanisms, J. Volcanol. Geotherm. Res., 90, 3-4, 263-280, doi:10.1016/S0377-0273(99)00024-4.

Cole, R. H. (1948). Underwater Explosions, Princeton University Press.

Cordonnier, B., E. Lev and F. Garel (2016). Benchmarking lava-flow models, Geol. Soc. Spec. Publ., 426, 1, 425-445, doi:10.1144/SP426.7.

Crespo, A. J. C., M. Gómez-Gesteira and R. A. Dalrymple (2007). Boundary Conditions Generated by Dynamic Particles in SPH Methods, Comput. Mater. Contin., 5, 3, 173-184, doi:10.3970/cmc.2007.005.173.

Dietterich, H. R. and K. V. Cashman (2014). Channel networks within lava flows: Formation, evolution, and implications for flow behavior, J. Geophys. Res. Earth Surf., 119, 8, 1704-1724, doi:10.1002/2014JF003103.

Fuchs, S. L., C. Meier, W. A. Wall and C. J. Cyron (2021). An SPH framework for fluid-solid and contact interaction problems including thermo-mechanical coupling and reversible phase transitions, Adv. Model. Simul. Eng. Sci., 8, 1, 15, doi:10.1186/s40323-021-00200-w.

Gingold, R. A. and J. J. Monaghan (1977). Smoothed particle hydrodynamics: theory and application to non-spherical stars, Mon. Not. R. Astron. Soc., 181, 3, 375-389, doi:10.1093/mnras/181.3.375.

Groulx, D. and W. Ogoh (2010). Thermal Behavior of Phase Change Material During Charging Inside a Finned Cylindrical Latent Heat Energy Storage System: Effects of the Arrangement and Number of Fins. 2010 14th International Heat Transfer Conference, 7, 417-424, doi:10.1115/IHTC14-22397.

Hérault, A. (2008). Création d'un système d'information pour la gestion des risques volcaniques, Volcanic risk assesment information system design, PhD, University of Paris-Est, https://dblp.org/rec/phd/hal/Herault08.html.

Hérault, A., G. Bilotta and R. A. Dalrymple (2010). SPH on GPU with CUDA, J. Hydraul. Res., 48, sup. 1, 74-79, doi:10.1080/00221686.2010.9641247.

Hérault, A., G. Bilotta, A. Vicari, E. Rustico et al. (2011). Numerical simulation of lava flow using a GPU SPH model, Ann. Geophys., 54, 5, doi:10.4401/ag-5343.

Kauahikaua, J., K. V. Cashman, T. N. Mattox, C. C. Heliker et al. (1998). Observations on basaltic lava streams in tubes from Kilauea Volcano, island of Hawai'i, J. Geophys. Res. Solid Earth, 103, B11, 27303-27323, doi:10.1029/97JB03576.

Lucy, L. B. (1977). A numerical approach to the testing of the fission hypothesis, Astron. J., 82, 1013, doi:10.1086/112164.

Molteni, D. and A. Colagrossi (2009). A simple procedure to improve the pressure evaluation in hydrodynamic context using the SPH, Comput. Phys. Commun., 180, 6, 861-872, doi:10.1016/j.cpc.2008.12.004.

Monaghan, J. J. (1994). Simulating Free Surface Flows with SPH, J. Comput. Phys, 110, 2, 399-406, doi:10.1006/jcph.1994.1034.

Monaghan, J. J. (2005). Smoothed particle hydrodynamics, Rep. Prog. Phys., 68, 8, 1703-1759, doi:10.1088/0034-4885/68/8/R01.

Rustico, E., G. Bilotta, G. Gallo, A. Herault et al. (2012). Smoothed Particle Hydrodynamics Simulations on Multi-GPU Systems. 2012 20th Euromicro International Conference on Parallel, Distributed and Network-Based Processing, 384-391, doi:10.1109/PDP.2012.21.

Saikali, E., G. Bilotta, A. Hérault and V. Zago (2020). Accuracy Improvements for Single Precision Implementations of the SPH Method, Int. J. Comput. Fluid Dyn., 34, 10, 774-787, doi:10.1080/10618562.2020.1836357.

Wendland, H. (1995). Piecewise polynomial, positive definite and compactly supported radial functions of minimal degree, Adv. Comput. Math., 4, 1, 389-396, doi:10.1007/BF02123482.

Zago, V. (2019). Smoothed Particle Hydrodynamics method and flow dynamics: the case of lava numerical modeling and simulation, University of Catania, https://hdl.handle.net/20.500.11769/582728.

Zago, V., G. Bilotta, A. Cappello, R. Dalrymple et al. (2017). Simulating Complex Fluids with Smoothed Particle Hydrodynamics, Ann. Geophys., 60, 6, sup.1, doi:10.4401/ag-7362.

Zago, V., G. Bilotta, A. Cappello, R. Dalrymple et al. (2018). Preliminary validation of lava benchmark tests on the GPUSPH particle engine, Ann. Geophys., 61, 2, doi:10.4401/ag-7870.

Zago, V., G. Bilotta, A. Hérault, R. A. Dalrymple et al. (2018). Semi-implicit 3D SPH on GPU for lava flows, J. Comput. Phys., 375, 854-870, doi:10.1016/j.jcp.2018.07.060.

Zago, V., R. A. Dalrymple, N. Almashan, G. Bilotta et al. (2023). Characterization and modeling of greenwater overtopping of a sea-level deck, Ocean Eng., 275, 114131, doi:10.1016/j.oceaneng.2023.114131.

Zago, V., L. J. Schulze, G. Bilotta, N. Almashan et al. (2021). Overcoming excessive numerical dissipation in SPH modeling of water waves, Coast. Eng., 170, 104018, doi:10.1016/j.coastaleng.2021.104018.

***CORRESPONDING AUTHOR: Vito ZAGO**,
Istituto Nazionale di Geofisica e Vulcanologia, Osservatorio Etneo, Catania, Italy
e-mail: vito.zago@ingv.it